Ignition kernel development and subsequent flame propagation in a planar methane/air turbulent jet

C. Turquand d'Auzay†, S.F. Ahmed‡, N. Chakraborty†
† *School of Engineering, Newcastle University, Newcastle Upon-Tyne, NE1 7RU, United Kingdom*
‡ *Department of Mechanical and Industrial Engineering, College of Engineering, Qatar University, P. O. Box 2713, Doha, Qatar*

1 Introduction

The localised forced ignition (spark, laser) of flammable mixtures is a topic of fundamental importance in combustion science. A thorough knowledge of ignition is needed for safety standards as well as in the design of efficient and reliable injection systems in automotive engines, in which misfire causes ineffective combustion. The relight of gas turbine in altitude would also benefit from an increased understanding of this phenomenon. The ignition of turbulent flammable mixtures is not only influenced by the minimum ignition energy or the critical flame radius, but it also is strongly dependent on the local properties reigning within the energy deposition region (turbulence characteristics, scalar gradients, mixture composition, etc.) and of the overall flow field.

Thanks to its simple geometrical configuration, jet flow ignition has been experimentally extensively analysed in terms of ignition and probability, flame evolution, propagation and eventually stabilisation. Detailed experimental measurements of the ignition probability have been performed by Ahmed and Mastorakos [1] for different operating conditions, and focused mainly on the flame kernel growth, and subsequent upstream flame propagation and stabilisation, when applicable. Ahmed and Mastorakos [1] also shown the importance of the edge flame mechanism in the flame development by measuring the flame propagation speed after ignition until its stabilisation. This experimental database has been extensively used to examine ignition models within the Large Eddy Simulation (LES) and Reynolds-Averaged Navier Stokes (RANS) frameworks. However, very few numerical studies have been directed to the fundamental understanding of the flame kernel evolution after localised forced ignition in shear-generated turbulence and inhomogeneous mixtures in which numerous flame regimes co-exist.

The present work aims to bridge this gap in the literature by discussing the extension of the current understanding of ignition gained from earlier DNS analysis in homogeneous and inhomogeneous mixtures under isotropic decaying turbulence, to turbulent inhomogeneous flows driven by shear. This is achieved by investigating the spark ignition of a planar methane-air jet using three-dimensional Direct Numerical Simulation (DNS) with modified single-step chemistry. The main objective of this work is to understand and extract the key physical phenomena driving the success or failure of a turbulent planar jet ignition.

Correspondence to: nct92@ncl.ac.uk

2 Numerical approach

Building on previous numerical analysis of ignition [8], a single step chemical mechanism (Fuel$+s$Oxidiser $\rightarrow (1+s)$Products, where s is the oxidiser/fuel ratio) has been used here in which the chemical source term is given by an Arrhenius law. To recover a realistic dependence of the laminar flame speed with the equivalence ratio, the correction proposed by Fernández-Tarrazo [3] was used, in which both the activation energy and the heat of combustion are functions of the local composition.

All the species are considered as calorically perfect gases with equal heat capacities at constant pressure. The species diffusion velocity is accounted for by using Ficks law, and the transport properties such as viscosity (μ), thermal conductivity (λ) and density weighted mass diffusivity (ρD) are similar and independent of temperature for all species. Furthermore, the Lewis number of all species is assumed to be unity.

The local mixture composition is characterised in terms of mixture fraction defined such that $\xi_j = 1$ and $\xi_c = 0$, yielding $\xi = (Y_{\mathrm{CH_4}} - Y_{\mathrm{O_2}}/s + Y_{\mathrm{O_2},c}/s)/(Y_{\mathrm{CH_4},j} - Y_{\mathrm{O_2},j}/s + Y_{\mathrm{O_2},c}/s)$, where $(.)_j$ and $(.)_c$ refer to jet and coflow quantities respectively. The stoichiometric mixture fraction is thus defined as $\xi_{\mathrm{st}} = (Y_{\mathrm{O_2},c}/s)/(Y_{\mathrm{CH_4},j} - Y_{\mathrm{O_2},j}/s + Y_{\mathrm{O_2},c}/s)$. The extent of the chemical reaction completion is measured by a reaction progress variable c that increases monotonically from zero in the reactants to unity in the products. It may be expressed as a function of the local fuel mass fraction, following $c = (Y^m_{\mathrm{CH_4}}(\xi) - Y_{\mathrm{CH_4}})/(Y^m_{\mathrm{CH_4}}(\xi) - Y^{\mathrm{eq}}_{\mathrm{CH_4}}(\xi))$, where $(.)^m$ and $(.)^{\mathrm{eq}}$ indicate the mixing and equilibrium values of the fuel mass fraction at the local mixture fraction as given by the Burke-Schumann diagram [6].

The effects of the localised forced ignition are accounted for by the addition of a source term in the energy equation (q''') that is Gaussian in space and step-wise in time [8]. The energy deposition is defined by three parameters, *(i)* its total energy E_{sp}, *(ii)* its characteristic width R_{sp} expressed as a function of the Zel'dovich flame thickness $\delta_z = D_0/s^0_l$ where s^0_l is the adiabatic stoichiometric methane/air unstrained laminar flame speed and D_0 the reactants mass diffusivity and *(iii)* its duration t_{sp} expressed as a fraction of the chemical time scale $t_f = \delta_z/s^0_l$.

3 Configuration and computational set-up

It should be noted, that the experimental work considered a round jet while the a slot jet was used in the present DNS analysis, as it is computationally much more affordable. A round jet indeed requires a larger domain to accommodate jet spreading in two directions.

The simulations have been carried out with the compressible 3D DNS code `SENGA+` [8]. The code employs a 10-th order central difference scheme for the internal points that gradually decreases to a one-sided 2nd-order scheme at the non-periodic boundaries for the spatial differentiation. The time advancement is carried out using a 3rd-order low-storage Runge-Kutta scheme.

The jet slot width is $h = 5.3\delta_{\mathrm{th}}$ (where $\delta_{\mathrm{th}} = [T_{\mathrm{ad}} - T_0]/\max(|\nabla\hat{T}|)$ is the thermal flame thickness and where $\hat{T}$, T_{ad} and T_0 are the dimensional instantaneous, stoichiometric adiabatic methane/air flame and reactants temperatures respectively), while the computational domain is long and wide enough to accommodate both the development of the flame kernel downstream of the ignition location and the mixing. Its dimensions are $L_{\mathrm{x}} \times L_{\mathrm{y}} \times L_{\mathrm{z}} \approx 37h \times 19h \times 4.3h$ and it is discretised with $1920 \times 990 \times 225$ uniform cubic cells of size Δx, leading to the slot width spanning 52 cells. This resolution ensures that δ_{th} is discretised by about 10 grid points, and that $\eta_k/\Delta\mathrm{x} > 1$ where η_k is the Kolmogorov length scale. The boundaries of the domain are periodic in the transverse directions (y and z in this work) and partially non-reflecting in the

stream-wise direction (x). The non-periodic boundaries are specified using the Navier-Stokes Characteristic Boundary Conditions (NSCBC) technique.

The fuel is injected through the slot with a bulk velocity $U_j = 40 s_l^0$ and issues in a coflow of air moving at a velocity $U_c = 0.1 U_j = 4 s_l^0$. The jet Reynolds number is $\mathrm{Re} = \rho_0 U_j h / \mu = 650$, where ρ_0 denotes the unburned gas density. At the inflow plane, the coflow is considered laminar without any added velocity perturbation, while within the slot, the velocity is imposed by scanning a plane through a frozen periodic fully developed turbulent channel flow with a scanning velocity U_j.

The mixture injected through the slot is composed of 27.5% of methane and 72.5% or air per volume, leading to $s = 4$, $Y_{\mathrm{O}_2,j} = 0.1925$, $Y_{\mathrm{CH}_4,j} = 0.1738$ and $\xi_{\mathrm{st}} = 0.312$, while the oxidiser mass fraction in air is $Y_{\mathrm{O}_2,c} = 0.233$. The mixture fractions corresponding to the rich and lean flammability limits are respectively $\xi_{\mathrm{rich}} = 0.4906$ and $\xi_{\mathrm{lean}} = 0.1943$. Both the jet and the coflow are preheated such that $\tau = (T_{\mathrm{ad}} - T_0)/T_0 = 4.5$ while standard values have been chosen for the Prandtl number ($\mathrm{Pr} = 0.7$) and the ratio of specific heat ($\gamma = 1.4$).

The width and duration of the energy deposition are kept constant in this work with $R_{\mathrm{sp}}/\delta_z = 2.45$, $t_{\mathrm{sp}} = 0.2 t_f$ and $E_{\mathrm{sp}} = 7.5(4/3)\pi\delta_z^3 \rho_0 C_p \tau T_0$. Two different energy deposition locations are selected, one on the centreline at $x/h = x^+ = 15$ and $z/h = z^+ = 0$ and one off-axis in the outer shear layer at $x^+ = 10$, $y/h = y^+ = -1$ and $z^+ = 0$ referred to respectively as $s1$ and $s2$ and visible in Fig. 1. The first is positioned upstream of the location $\tilde{\xi} > \xi_{\mathrm{rich}}$ (where $\tilde{\xi} = \overline{\rho\xi}/\bar{\rho}$ is the Favre averaged mixture fraction), while the second is positioned at $\tilde{\xi} \approx \xi_{\mathrm{st}}$. The flammability factor (defined as $\mathcal{F} = \int_{\xi_{\mathrm{lean}}}^{\xi_{\mathrm{rich}}} \mathrm{P}(\eta)\,\mathrm{d}\eta$ in Ref. [2]) values at both locations are comparable with $\mathcal{F} \leqslant 0.5$. Finally, for both energy depositions, the instantaneous value of the mixture fraction at the centre of the ignitor is within the flammability range. The effect of the local instantaneous mixture fraction at the energy deposition location on the flame kernel development and ignition success rate will form the basis of future investigations.

The DNS simulations have been initially carried out in non-reacting mode for about two flow-through times ($t_j = L_{\mathrm{x}}/(0.5(U_j + U_c))$) such that the initial transients disappear and that realistic fluctuations of mixture composition and velocity are established. The obtained flow field is then used as the initial condition for the energy deposition which occurs at $t/t_{\mathrm{sp}} = t^+ = 0$. The following reacting simulations last as long as necessary to either observe a kernel quenching, the kernel leaving the domain (i.e. blow-out) or the onset of flame stabilisation (i.e. flame propagating upstream).

4 Results and discussion

The mean mixture fraction and flammability factor fields are shown in Fig. 1, along with isolines of mixture fraction corresponding to $\tilde{\xi}_{\mathrm{lean}}$, $\tilde{\xi}_{\mathrm{st}}$ and $\tilde{\xi}_{\mathrm{rich}}$ respectively. The $\tilde{\xi} = \tilde{\xi}_{\mathrm{rich}}$ isoline closes along the centreline at about $x^+ \approx 20$, indicating that the whole mixture downstream is flammable (in a mean sense). The flammability factor is also shown and measures the probability of finding a flammable mixture at any given time, which is linked with the flapping frequency of the jet. It is zero near the inflow due to the very rich nature of the mixture injected, although its value in the outer shear-layers is non-zero thanks to shear-generated mixing. Its value increases downstream which is caused by the mixing of the fuel-rich mixture from the jet with the pure air of the coflow. This mixing decreases the mixture fraction until $\mathcal{F}$ reaches unity near the centreline far downstream of the nozzle lip ($x^+ \geqslant 35$) indicating that irrespective of the instantaneous flow configuration, the mixture found will be flammable. This indicates that any flame front upstream of $x^+ \approx 30$ will find conditions more and more favourable to burning as it propagates downstream.

The development of the kernel $s2$ after energy deposition is shown in Fig. 2 using the non-dimensional

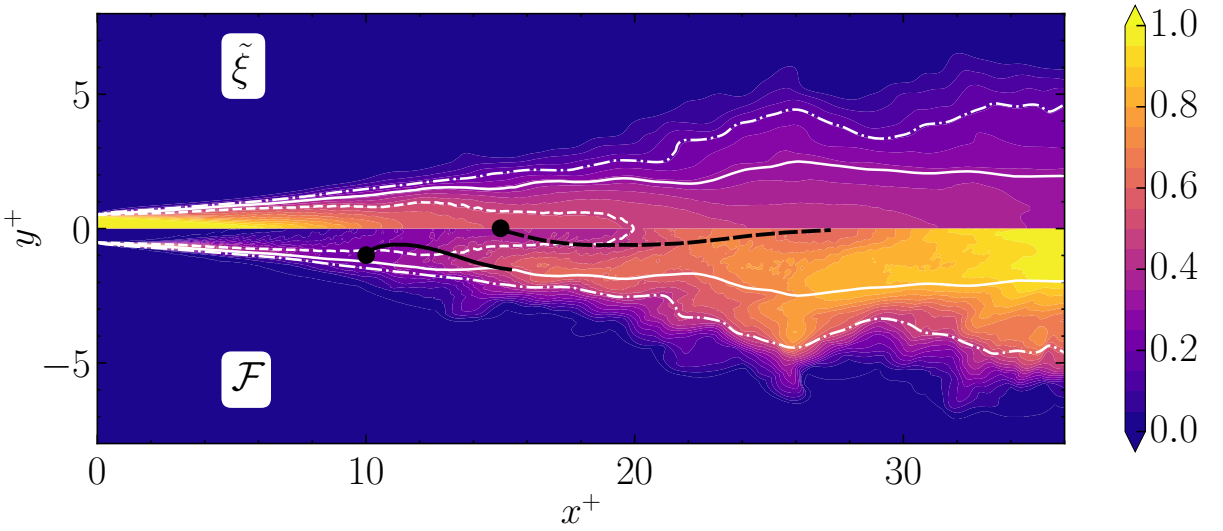

Figure 1: *(top)* Favre-averaged mixture fraction ($\tilde{\xi}$) and *(bottom)* flammability factor ($\mathcal{F}$) fields, with the iso-contours of *(plain lines)* $\tilde{\xi}_{\text{st}}$, *(dashed lines)* $\tilde{\xi}_{\text{rich}}$ and *(dash-dotted lines)* $\tilde{\xi}_{\text{lean}}$ - The kernels mass centre positions in time are overlaid in black lines for ignition locations *(plain)* $s1$ and *(dashed)* $s2$

temperature $T = (\hat{T} - T_0)/(T_{\text{ad}} - T_0)$ field. Shortly after the energy deposition, a kernel that is still confined near the energy deposition location is visible, while the flame present a fully-premixed type behaviour driven by the large temperature values resulting from the energy deposition. The flame kernel is then convected downstream by the local turbulent velocity field, while it starts to grow. This initial growth is driven by the very large gradient of temperature. At $t^+ \approx 6$, its growth becomes supported by the formation of multiple triple flames that propagates along the stoichiometric mixture fraction iso-surface, with the presence of both rich and lean premixed flames and that of a diffusion flame stabilised along the ξ_{st} iso-surface. The growth rate in the stream-wise direction is rather small, while the kernel develops more rapidly in the homogeneous (z) direction. This is explained by the presence of relatively large values of the stream-wise scalar gradient around the energy deposition location, and lower values in the homogeneous direction, and by the fact that these large values of the scalar gradient detrimentally affect the edge flame speed [4]. By $t^+ = 15.2$, the flame kernel has significantly moved downstream of the ignition location, and develops in a region where the scalar gradients are smaller and the mixture fraction closer to its stoichiometric value. Both these factors contribute positively to an increased growth rate, resulting in a larger and larger kernel as time progresses. The formation of multiple pockets can also be noted, in which some are due to out-of-the-plane motion of the flame, while others are due to the diffusion of temperature through the regions in which the mixture is either too rich or too lean to allow flame development, leading to the creation of new regions of burning.

By comparing the visualisations at $t^+ \approx 28$ and at $t^+ \approx 40$, the flame leading edge visibly stabilises which suggests some anchoring of the flame in the outer shear layer (i.e. $(x^+, y^+) \approx (20, -5)$). As the theoretical laminar edge flame speed is $s_e = s_l^0\sqrt{1+\tau} \approx 2.35 s_l^0$ [7], it becomes possible for the flame to locally propagate faster than the local flow field, or as least stabilise as the stream-wise component of the velocity in this region is close to that of the coflow ($4s_l^0$) and may locally becomes negative in the large roll-ups visible in the two shear layers present on both sides of the nozzle. This is further confirmed by Fig. 3(a), that presents the extent of the flame in the stream-wise direction, for ignition location $s2$ and $t^+ \geqslant 25$.

Figure 3(a) also shows that the kernel resulting from the energy deposition at location $s1$ did not survive

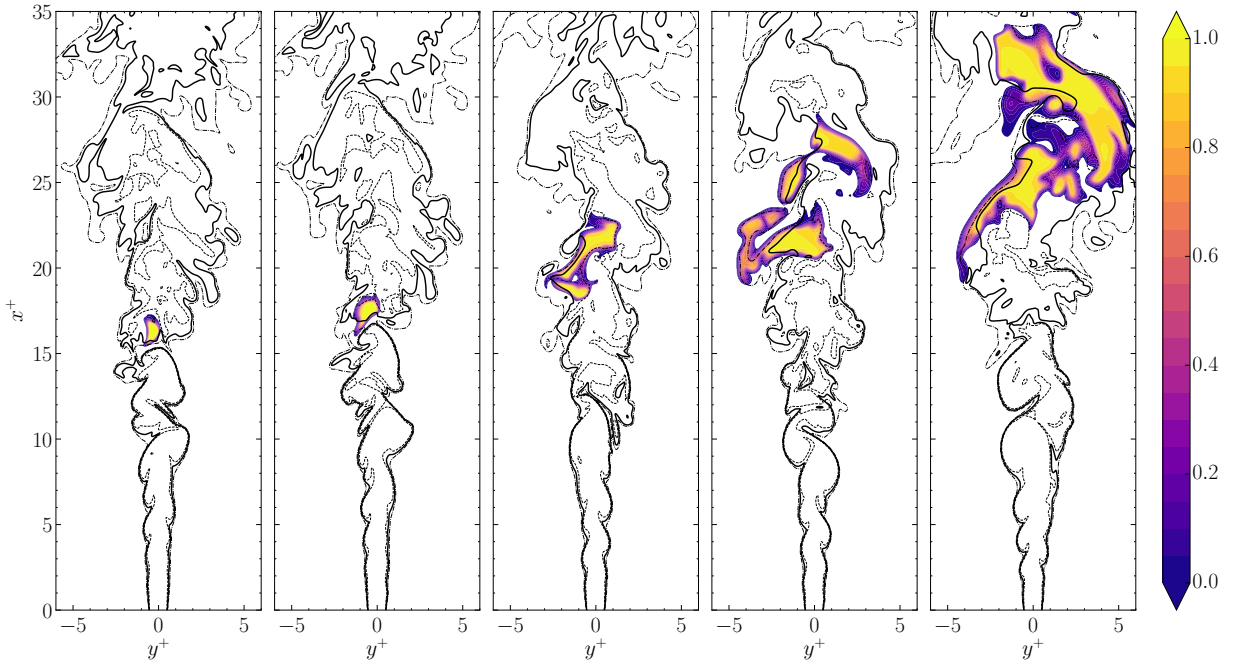

Figure 2: Time evolution of T overlaid with *(plain line)* ξ_{st}, *(dashed line)* ξ_{rich} and *(dash-dotted line)* ξ_{lean} for ignition point $s2$ at *(from left to right)* $t^+ = 4,\ 7.2,\ 15.4,\ 27.6,\ 40$

past $t^+ \approx 18$ and quenched. A closer examination of the temporal evolution of the burned gas volume (measured by the volume contained within the iso-surface $c = 0.5$ and not shown here for brevity) for this event indicates that it stopped growing at $t^+ \approx 10$.

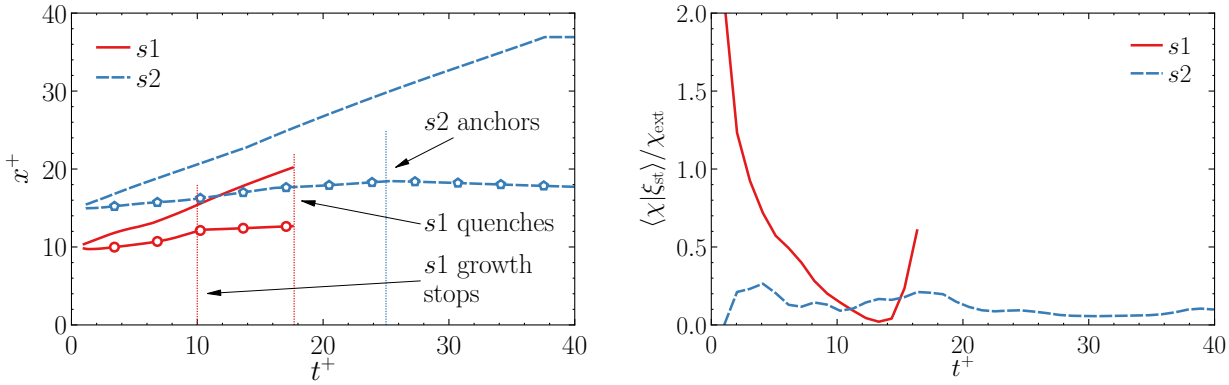

Figure 3: Time evolution of *(left)* the flame *(symbols)* leading and *(lines)* trailing edges axial position (located with $c = 0.1$) *(right)* the scalar dissipation rate along the edge flame ($\langle\chi|\xi_{\text{st}}\rangle/\chi_{\text{ext}}$)

To explain the occurrence of such different outcomes after an identical amount of energy has been deposited on comparable mixture fraction iso-surfaces, it is instructive to investigate the reaction zone statistics and in particular the scalar dissipation rate on the flame front. The temporal evolution of the mean normalised scalar dissipation rate (SDR) measured on the edge flame ($\langle\chi|\xi_{\text{st}}\rangle/\chi_{\text{ext}}$ where $\chi = 2D(\nabla\xi)^2$ is the SDR

and $\chi_{\text{ext}} = \xi_{\text{st}}^2(1-\xi_{\text{st}})^2/t_f$ its extinction value as defined by Peters [5]) is thus shown in Fig. 3(b) for both ignition locations. It is clear that the SDR value along the edge flame is much larger for the kernel $s1$ than for $s2$, where the mean takes values larger than the extinction limit. Although a large scatter of the SDR values is observed at all times (not shown here for brevity), this means that during most of its lifespan, the kernel $s1$ develops in conditions which are not conducive to the edge flame propagation and thus to flame kernel growth, which eventually leads to flame quenching. On the other hand, the kernel $s2$ propagates in regions of the jet where the scalar gradients are much smaller, and is thus able to grow much more readily.

5 Conclusions

The localised forced ignition and subsequent flame propagation in a planar turbulent methane jet in ambient air has been simulated using Direct Numerical Simulation (DNS) with a modified single-step chemistry. Two different ignition locations were considered using identical energy deposition parameters (duration, width, total energy). The kernels formation and subsequent growth leading to either flame propagation or quenching were analysed. The current DNS framework captures these two outcomes reasonably well. Following ignition, and after a short time in which the kernel growth is driven by the large temperature gradient resulting from the energy deposition, it is found that the flame presents a tribrachial structure in which the triple-point propagates along the stoichiometric iso-surface. At early times, the convection dominates the movement of the flame kernel leading edge, resulting in the flame being advected downstream. If a self-sustained flame state is to be obtained in which the flame is stabilised, the propagation of the flame leading edge locally need to reach an equilibrium with the local stream-wise velocity. Finally, the key role played by the scalar dissipation rate (SDR) is highlighted by showing that the quenching of the first kernel results from the mean SDR along its edge flame front being above the extinction limit.

Acknowledgements

The authors are grateful to the British Council for financial support and to EPSRC (ARCHER, Cirrus) and Newcastle University (Rocket) for computational support

References

[1] Ahmed S.F., Mastorakos, E. (2006), Spark ignition of lifted turbulent jet flames, Combust. Flame 146:215
[2] Birch A.D. et al. (1981), Ignition probabilities in turbulent mixing flows, Proc. Combust. Inst. 18:1775
[3] Fernandez-Tarrazo E. et al. (2006), A simple one-step chemistry model for partially premixed hydrocarbon combustion, Combust. Flame 147:32
[4] Pantano C. (2004), Direct simulation of nonpremixed flame extinction in methane-air jet with reduced chemistry, J. Fluid Mech. 514:231
[5] Peters N. (2000), Turbulent Combustion, 1st edition, Cambridge University Press
[6] Poinsot T., Veynante D. (2005), Theoretical and Numerical Combustion, 2nd edition, Edwards
[7] Ruetsch G.R., et al. (1995), Effects of heat release on triple flames, Phys. Fluids, 7(6):1447
[8] Turquand d'Auzay C. et al. (2019), On the minimum ignition energy and its transition in the localised forced ignition of turbulent homogeneous mixtures, Combust. Flame 201:104